catalysts

MDPI

Article

Enhanced C2 and C3 Product Selectivity in Electrochemical CO_2 Reduction on Carbon-Doped Copper Oxide Catalysts Prepared by Deep Eutectic Solvent Calcination

Melanie Iwanow [1,2], Johannes Seidler [1], Luciana Vieira [1], Manuela Kaiser [1], Daniel Van Opdenbosch [3], Cordt Zollfrank [3], Tobias Gärtner [4], Michael Richter [1], Burkhard König [2] and Volker Sieber [1,3,*]

1 Fraunhofer Institute for Interfacial Engineering and Biotechnology IGB, Bio-, Electro- and Chemocatalysis BioCat, Straubing Branch, Schulgasse 11a, 94315 Straubing, Germany; melanie.iwanow@igb.fraunhofer.de (M.I.); johannes.seidler@igb-extern.fraunhofer.de (J.S.); luciana.vieira@igb.fraunhofer.de (L.V.); manuela.kaiser@igb.fraunhofer.de (M.K.); michael.richter@igb.fraunhofer.de (M.R.)
2 Department of Chemistry and Pharmacy, University of Regensburg, Universitätsstraße 31, 93040 Regensburg, Germany; burkhard.koenig@ur.de
3 Campus Straubing for Biotechnology and Sustainability, Technical University of Munich, Schulgasse 16, 94315 Straubing, Germany; daniel.van-opdenbosch@tum.de (D.V.O.); cordt.zollfrank@tum.de (C.Z.)
4 ESy Labs, An der Irler Höhe 3a, 93055 Regensburg, Germany; tobias.gaertner@esy-labs.de
* Correspondence: sieber@tum.de

check for updates

Citation: Iwanow, M.; Seidler, J.; Vieira, L.; Kaiser, M.; Van Opdenbosch, D.; Zollfrank, C.; Gärtner, T.; Richter, M.; König, B.; Sieber, V. Enhanced C2 and C3 Product Selectivity in Electrochemical CO_2 Reduction on Carbon-Doped Copper Oxide Catalysts Prepared by Deep Eutectic Solvent Calcination. *Catalysts* **2021**, *11*, 542. https://doi.org/10.3390/catal11050542

Academic Editor: David Sebastián

Received: 2 April 2021
Accepted: 20 April 2021
Published: 23 April 2021

Abstract: Copper and its oxides are the main catalyst materials able to promote the formation of hydrocarbons from the electrocatalytic CO_2 conversion. Herein, we describe a novel preparation method for carbon-doped copper oxide catalysts based on an oxidative thermal treatment of copper-containing deep eutectic solvents (DES). XRD and EDX analysis of the samples show that thermal treatment at 500 °C in air for a prolonged time (60 min) provides exclusively carbon-doped copper(II) oxide catalysts, whereas shorter calcination time leads to a mixture of less oxidized forms of copper (Cu_2O and Cu^0), CuO, and a higher carbon content from the DES. Chronoamperometry of the electrode containing the prepared materials in 0.5 M $KHCO_3$ electrolyte show the reduction of CuO to less oxidized copper species. The materials prepared by the use of different DES, copper precursors and calcination times were used as electrocatalysts for the electrochemical CO_2 reduction. Chemical analysis of the products reveals an enhanced selectivity toward C2 and C3 products for the catalyst prepared from the DES galactose-urea with copper nanoparticles and calcination for 60 min in air. The electrocatalytic activity of the prepared materials were compared to commercial CuO and showed a higher product concentration at −1.7 V vs. Ag/AgCl, with formation rates of 7.4, 6.0, and 10.4 μmol h^{-1} cm^{-2} for ethanol, n-propanol, and ethylene, respectively.

Keywords: copper oxide catalysts; catalyst preparation; calcination; deep eutectic solvents; electrochemical CO_2 reduction

1. Introduction

The rising concentration of global atmospheric carbon dioxide since the beginning of industrialization (280 parts per million by volume (ppmv) to 365 ppmv) [1] requires a reduction of carbon dioxide release and solutions for its capture and utilization [2–4]. Several technologies have been developed for CO_2 capture involving point sources or direct air capture [5]. As for the CO_2 utilization, using CO_2 for chemical synthesis of industrial relevant chemicals would be a sustainable solution not only for the utilization but also for the replacement of fossil-based chemicals by CO_2-neutral alternatives. In this way, the electrochemical reduction of CO_2 using directly renewable electricity is a promising conversion method toward carbon-neutral economy. The electrochemical carbon dioxide reduction (CO_2R) process can use CO_2 as a building block for the synthesis of

several value-added products. Moreover, CO_2R offers a possibility for storing intermittent renewable energy, such as wind and solar, since it would be in principle relatively simple to ramp up and down according to the energy availability [6–8].

Mild reaction conditions (ambient pressure and temperature) and the use of low-cost catalysts are key advantages of the electrocatalytic CO_2 conversion in aqueous media [9,10]. Nevertheless, the electrochemical CO_2 reduction takes place at rather negative potentials; hence, it competes with the hydrogen evolution reaction (HER). Therefore, a powerful catalyst is required to turn the onset potential more positive, favoring the CO_2 reduction and suppressing hydrogen production. Copper and its oxides (CuO and Cu_2O) are one of the few materials to catalyze the formation of C–C bonds and lead to alcohols and hydrocarbons [6,11–16]. The preparation method of the Cu-based catalysts or electrodes can have an effect on the selectivity of product formation. Depending on the potential, surface morphology, and oxidation state of the catalyst, a wide variety of products can be obtained in different ratios: carbon monoxide, methane, ethylene, methanol, ethanol, n-propanol, and formate (Table 1) [11–13,17].

Table 1. CO_2 reduction products on the cathode with their respective potentials at pH 7 [18,19].

Chemical Equations	Potential V vs. SHE
$CO_2 + H_2O + 2\,e^- \rightarrow HCOO^-(aq) + OH^-$	−0.43 V
$CO_2 + H_2O + 2\,e^- \rightarrow CO\uparrow + 2\,OH^-$	−0.52 V
$2\,CO_2 + 8\,H_2O + 12\,e^- \rightarrow C_2H_4\uparrow + 12\,OH^-$	−0.34 V
$2\,CO_2 + 9\,H_2O + 12\,e^- \rightarrow C_2H_5OH\,(aq) + 12\,OH^-$	−0.33 V
$3\,CO_2 + 13\,H_2O + 18\,e^- \rightarrow C_3H_7OH\,(aq) + 18\,OH^-$	−0.32 V

Herein, we report a novel and facile preparation method of carbon-doped copper oxide materials and its application as catalysts for electrochemical CO_2 reduction. The materials were prepared by a slight modification of the deep eutectic solvent (DES) pyrolysis method, previously described by our group [20,21]. The initial method is based on the pyrolysis of metal-containing DES in an inert nitrogen atmosphere, which led to metal embedded in a carbon support rich in oxygen and nitrogen functional groups ($metal^0$/CNO). Such Cu/CNO materials showed high selectivity for the production of formate in liquid phase from CO_2 electrolysis [21]. In the presented preparation method, the calcination atmosphere has been changed from N_2 to air, resulting in partially oxidized copper due to the oxidative conditions. These produced carbon-doped CuO resulted in higher selectivity for C2 (ethylene, ethanol) and C3 (n-propanol) molecules during electrochemical CO_2 reduction. Compared to commercial copper(II) oxide nanoparticles, the activities and selectivities of the as-prepared catalysts are significantly higher. Thus, we could tailor this facile synthesis method to improve the productivity and selectivity of the catalysts. The influence of calcination time (10, 15, or 60 min) in the oxidative atmosphere as well as the influence of different deep eutectic solvents and copper precursors on the catalytic activity of the prepared materials were investigated in detail.

2. Results and Discussion

2.1. Catalyst Synthesis and Material Characterization

Carbon-doped copper oxide materials were produced by systematically varying the preparation parameters such as type of DES, copper precursor, pre-treatment atmosphere, calcination time, and temperature. The pre-treatment step was carried out in an inert or air atmosphere for 1.5 h. This step enables a homogeneous and controlled thermal treatment of the copper-containing DES under stirring. After pre-heating, the resulting solid mixture is transferred to an evaporating dish and calcined in a muffle furnace under air or N_2. Pyrolysis under inert gas leads to a final mixture of metallic copper in a considerable amount of carbon support prevenient of the DES (Cu/CNO) [21]. Calcination in air leads

to a considerably lower content of CNO due to the total oxidation of the DES molecules and its release as gases, as well as to the oxidation of the copper species to CuO. In this work, we have focused on the calcination in air for the preparation of carbon-doped CuO. These materials were further used as catalysts for electrochemical CO_2 reduction.

The catalyst Cu-a, prepared with the DES glucose-urea (Glc-U) and copper nanoparticles (CuNP), pre-treated and calcined for 60 min at 500 °C in air, was set as benchmark. Following materials were prepared, changing the DES to galactose-urea (Gal-U, Cu-b), the copper precursor to CuO (Cu-c), the calcination time to 15 min in air (Cu-d), or the pre-treatment atmosphere to nitrogen (Cu-g). Since the remaining supporting material (CNO) can influence the catalyst activity [21], the preparation method was slightly modified for Cu-e and Cu-f in order to increase the amount of CNO in the final material. Cu-e and Cu-f were first pre-treated under nitrogen. After cooling to room temperature, the mixture was transferred to an oven and heated up to 450 °C (Cu-e) or 500 °C (Cu-f), also under nitrogen atmosphere. Subsequently, the atmosphere was changed to air and the temperature was raised to 500 °C (Cu-e) or 550 °C (Cu-f) and kept for 10 min. In this way, carbon-supported copper oxide catalysts (CuO/CNO) should be obtained (Table 2).

Table 2. Overview of the different preparation parameter. The following abbreviations correspond to Glc-glucose, Gal-galactose, U-urea, CuNP-copper nanopowder, RT-room temperature. Cu-e and Cu-f were prepared in two steps: pyrolysis under inert atmosphere and oxidative treatment for 10 min. The CuO-60 catalysts are Cu-a, Cu-b, Cu-c, and Cu-g.

	Precursor		**Pre-Treatment**			**Calcination**		
	DES	**Metal**	***t* [h]**	***T* [°C]**	**Atm.**	***t* [min]**	***T* [°C]**	**Atm.**
Cu-a	Glc-U	CuNP	1.5	290	air	60	500	air
Cu-b	Gal-U	CuNP	1.5	290	air	60	500	air
Cu-c	Glc-U	CuO	1.5	290	air	60	500	air
Cu-d	Glc-U	CuNP	1.5	290	air	15	500	air
Cu-e	Glc-U	CuNP	1.5	290	N_2	from RT 10	to 450 500	N_2 air
Cu-f	Glc-U	CuNP	1.5	290	N_2	from RT 10	to 500 550	N_2 air
Cu-g	Glc-U	CuNP	1.5	290	N_2	60	500	air

The morphologies and elemental compositions of the prepared materials were analyzed by SEM and EDX. Figure 1-I shows the SEM images for Cu-b (a) and Cu-f (b). Cu-b was calcined in air only, whereas Cu-f was thermally treated in two steps, first in nitrogen then in air atmosphere. Figure 1-II gives an overview of the elemental composition of all materials investigated by EDX analysis. Catalysts prepared by 60 min calcination in air (Cu-a, Cu-b, Cu-c, and Cu-g) exhibit in general a quite homogeneous morphology, as shown in Figure 1-Ia for Cu-b and in Figure S2 in the Supplementary Material for all investigated materials. EDX analysis reveals that Cu-b is rich in copper with a low content of carbonaceous supporting material, similarly to Cu-a, Cu-c, and Cu-g. The copper content in these materials lay between 72.8 and 80.3 wt% with less than 6.6 wt% of CNO.

Catalysts Cu-d, Cu-e, and Cu-f with a shorter thermal treatment in air (10 or 15 min in air) show different particle morphology compared to Cu-a, Cu-b, Cu-c, and Cu-g, as depicted in the SEM image in Figure 1-Ib and Figure S2 in the Supplementary Material. EDX of the catalyst Cu-d, Cu-e, and Cu-f, which were first thermally treated in an inert atmosphere, reveals a higher concentration of carbonaceous material compared to samples treated in air only. EDX analysis shows different composition for the different particle types: (+) CuO domains with less carbon support; and (−) CuO/CNO domains with comparable lower copper contents (<50 wt%) and higher amounts of supporting material consisting of carbon, nitrogen, and oxygen. Thus, varying thermal treatment time in oxygen-containing

atmosphere changes the ratio of Cu/C/N/O. Shorter thermal treatment time in air leads to more remaining CNO support, whereas longer pyrolysis in air mostly oxidizes the material to CuO and converts the remaining DES to CO_2. Nevertheless, the final material did not result in a homogeneous composition, indicating heterogeneous oxidation of the catalysts. More details on the preparation method and elemental composition can be found in Table 6 Section 3.1.

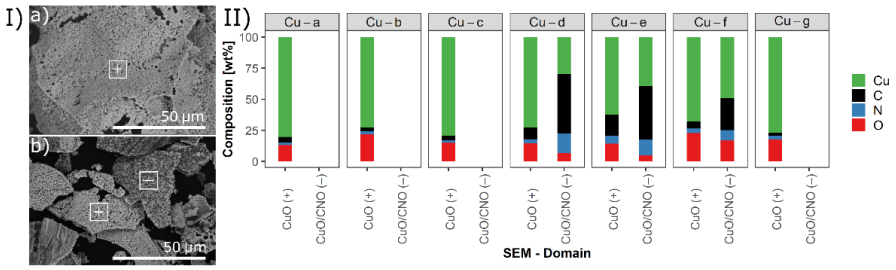

Figure 1. (**I**) SEM images of (a) Cu-b and (b) Cu-f. (**II**) Elemental composition (EDX) of synthesized copper catalysts Cu-a, Cu-b, Cu-c, Cu-d, Cu-e, Cu-f, and Cu-g.

Varying the copper precursor also influences the morphology of the synthesized materials. Copper nanoparticles < 100 nm (Cu-a, Cu-b, Cu-d, Cu-e, Cu-f, and Cu-g) led to a frilled and compact structure with smooth surfaces (Cu-a in Figure 2a), while CuO < 50 nm as precursor led to larger pores and less dense ordered structure (Cu-c, Figure 2b). The different size of the used metal precursor particles may have affected the surface of the materials. Moreover, calcination at 500 °C may lead to sintering of the copper(II) oxide in Cu-c. In addition, the carbon-rich domains of the catalysts Cu-d, Cu-e, and Cu-f (CuO/CNO) show a similar smooth morphology compared to the Cu/CNO materials synthesized previously [21]. SEM images of all prepared catalysts are shown in Figure S3 in the Supplementary Material.

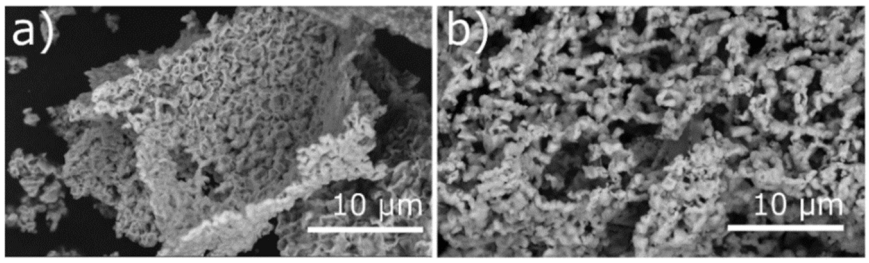

Figure 2. SEM images of (**a**) Cu-a and (**b**) Cu-c. Cu-a shows a frilled and compact CuO structure obtained from CuNP precursor, and Cu-c shows large pores and a less dense ordered structure from CuO as precursor.

The effect of the annealing time and atmosphere on the oxidation of copper was additionally investigated by X-ray powder diffractometry (XRD). Different oxidation states of copper (0, + I, + II) can be observed from the reflexes (Figure S4, Supplementary Material). Cu-a, Cu-b, Cu-c, and Cu-g only show reflexes attributed to copper(II) oxide and are, therefore, abbreviated in the following text as CuO-60 catalysts, due to the 60 min oxidative treatment. XRD of samples prepared with shorter treatment time in an O_2-containing atmosphere (Cu-d, Cu-e and Cu-f) show reflexes of less oxidized forms of copper, such as Cu_2O and Cu^0, besides CuO. Thus, longer treatment times in an O_2-containing atmosphere at 500 °C lead to higher-oxidized copper species.

By applying the Scherrer equation, crystallite sizes of CuO were examined [22]. The calculation of the crystallite sizes for the CuO-60 catalysts were performed as shown in the Supplementary Material (Figure S1) and are presented in real space in Table 3. Similar sizes of the crystallites were found regarding the x- and y-direction, with exception of the

Cu-c catalyst, which shows a clear deviation in x-direction with 69.2 nm instead of a length between 50.5 and 58.6 nm. However, the crystallites differ strongly in z-direction between 44.5 nm (Cu-a, Cu-c) and 89.3 or 96.0 nm for Cu-b and Cu-g, respectively. Interestingly, the copper precursor is not the only dimension-determining factor of the crystallites, because Cu-a (CuNP) and Cu-c (CuO) exhibit an equal length in z-direction. However, the used deep eutectic solvent seems to influence the length of the copper crystallites in z-direction.

Table 3. Crystallite sizes in x-, y-, and z-direction relative to the unit cells for the CuO-60 catalysts.

Catalyst	D_x [nm]	D_y [nm]	D_z [nm]
Cu-a	50.5	33.4	44.5
Cu-b	58.6	35.6	89.3
Cu-c	69.2	31.0	44.5
Cu-g	50.8	37.2	96.0

This is consistent with findings from Wagle et al. that DES can fulfil multiple roles in directing chemistry at the nanoscale and thus dictate growth along defined directions [23]. Cu-b was prepared with the DES Gal-U instead of Glc-U, and the preparation of Cu-g differs in the inert pre-treatment atmosphere compared to the catalysts Cu-a, Cu-b, and Cu-c. Thus, during the first step of the Cu-g catalyst preparation, resulting carbon-rich supporting material from DES is available and may influence the building of copper crystallites.

2.2. Electrochemical CO_2 Reduction

In order to prove that the products come solely from CO_2 reduction and not from the decomposition of the bicarbonate in the electrolyte or from remnants of the pyrolysis of the DES, an experiment with Cu-e in Helium-saturated 0.5 M $KHCO_3$ electrolyte was performed. Only hydrogen (164.5 µmol h^{-1} cm^{-2}) was produced in the absence of CO_2. Thus, neither the bicarbonate electrolyte nor remnants of the pyrolysis of the DES are involved in product formation. In helium-saturated electrolytes, water is the only redox species available for reduction on the catalyst active sites, whereas in CO_2-saturated solutions, water and CO_2 compete for the electrode reactions. The pH of the catholyte increases considerably during the reaction in both, He- and CO_2-saturated electrolytes (Table S1, Supplementary Material), due to the generation of OH^- ions from water reduction to hydrogen (Equation (1)) [24,25].

$$2\,H_2O + 2\,e^- \rightarrow H_2 \uparrow + 2\,OH^- \quad (1)$$

$$OH^- + HCO_3^- \rightarrow H_2O + CO_3^{2-} \quad (2)$$

$$CO_2 + H_2O \leftrightarrows (H_2CO_3) \leftrightarrows HCO_3^- + H^+ \quad (3)$$

$$2\,H_2O \rightarrow O_2 \uparrow + 4\,H^+ + 4\,e^- \quad (4)$$

In principle, the bicarbonate electrolyte could buffer the pH increase (Equation (2)). However, the electrolyte concentration (0.5 M $KHCO_3$) is rather low, and the pH rises [25]. The solubility of CO_2 in the bicarbonate electrolyte depends on the pH. In more acidic solutions, the solubility of CO_2 is higher, and the equilibrium in Equation (3) shifts toward HCO_3^-, whereas for pH values higher than 8, no diluted CO_2 is expected to be present [26]. To overcome the limitation of low CO_2 dissolution in aqueous solutions, experiments were carried out on gas-diffusion electrodes. Thereby, the supply of CO_2 to the catalyst surface was maintained by the transport of gaseous CO_2 through the gas-diffusion layer.

Catalysts prepared by varying the DES, copper precursor, and calcination times were coated on these gas-diffusion layers and measured toward their activity for CO_2 reduction. The parameters for the electrochemical CO_2 reduction in a three-compartment cell were optimized using the Cu-a and Cu-g catalyst as a benchmark. The experiments in 0.5 M $KHCO_3$ electrolyte with 5 mg cm^{-2} catalyst loading, a constant CO_2 gas flow of 10 mL min^{-1}, and a potential of −1.7 V vs. Ag/AgCl showed the highest product formation rates and were

used for comparison of the electrocatalytic activities of all prepared materials (Table S2, Figures S5 and S6, Supplementary Material). Higher-concentrated electrolytes (0.5 M instead of 0.1 M $KHCO_3$) showed higher product formation and a more stable electrochemical process (Table S2, Supplementary Material). In lower-concentrated electrolytes, the current density decreased more rapidly, due to lower conductivity and electro-decomposition. At the anode, water molecules of the anolyte are oxidized to molecular oxygen releasing protons (Equation (4)), and the equilibrium of carbonic acid (Equation (3)) shifts toward CO_2 and water.

Our experiments showed that after ~40 min in 0.1 M $KHCO_3$ the current density drops, and the anolyte had to be replaced. The same effect was observed only after ~120 min in 0.5 M $KHCO_3$ (Figure S7, Supplementary Material). Water oxidation to oxygen and the migration of potassium ions through the cation exchange membrane led to a decrease of electrolyte concentration, which reduces the conductivity and strongly increases cell resistance.

An initial assessment of the current densities at different applied potentials in CO_2-saturated 0.5 M $KHCO_3$ was carried out by linear sweep voltammetry (LSV) and chronoamperometry (CA) (Figure 3). A comparison of the measurements in CO_2- and Argon-saturated solutions for all catalysts is shown in Figure S8 in the Supplementary Material.

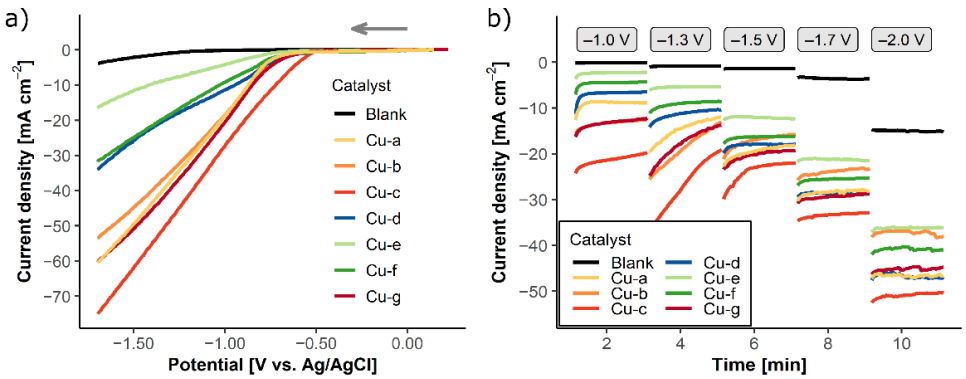

Figure 3. (**a**) LSV and (**b**) CA measurements of the synthesized copper catalysts in CO_2-saturated 0.5 M $KHCO_3$, blank = carbon paper without catalyst. LSV was measured from open circuit potential (OCP) to −1.7 V vs. Ag/AgCl. CA measurements were performed at the different step potentials −1.0, −1.3, −1.5, −1.7, and −2.0 V vs. Ag/AgCl for 2 min each.

LSV of the different copper catalysts in CO_2-saturated electrolytes shows higher current densities and more positive onset potentials (ΔE of 0.5–0.7 V vs. Ag/AgCl) compared to the carbon paper substrate (Figure 3a). The current densities differ depending on the preparation parameters. CuO-60 catalysts (Cu-a, Cu-b, Cu-c, and Cu-g) show quite high current densities (from 55 to 75 mA cm^{-2}) compared to the sample containing less oxidized copper (Cu-d, Cu-e, and Cu-f), which exhibit current densities between 17 and 34 mA cm^{-2}. In particular, Cu-c stands out with the highest current density of 75 mA cm^{-2} and the most positive onset potential at −0.5 V vs. Ag/AgCl. Based on the higher current densities and lower onset potentials, the CuO-60 catalysts could have higher activity toward CO_2 reduction.

In Figure 3b, the chronoamperometric profile of the different catalyst materials are shown in CO_2-saturated 0.5 M $KHCO_3$ electrolyte. CA allow the examination of the electrochemical stability of a catalyst in a certain potential for a longer time. In accordance with the LSV, all materials exhibit considerably high current densities (between ~30 and 50 mA cm^{-2} at −2.0 V vs. Ag/AgCl) compared to the carbon paper without catalyst (blank). At the investigated potentials −1.0 and −1.3 V vs. Ag/AgCl, the CuO-60 catalysts induce higher current densities. The current density of these catalysts at −1.3 V vs. Ag/AgCl is not constant during the two minutes of applied potential, and it drops with time. This current drop may be caused by the reduction of copper(II) oxide to less

oxidized copper species. Thus, the active catalyst in the CO_2 reduction is not the copper(II) oxide, but an oxide-derived less oxidized copper species, which is formed in situ during the electrode polarization. In the literature, it is already reported that oxide-derived copper catalysts are beneficial for the selectivity toward C2 and C3 product formation [27–32]. Yeo and coworkers found that copper oxide is preferably reduced to metallic copper at the same potential range of the CO_2 reduction, and metallic copper with a different morphology is formed during this reduction step, resulting in a rough surface with defects [32]. Lum et al. reported that −1.2 V vs. Ag/AgCl is used for the reduction of the oxide layer on the copper catalyst [27], which is consistent with the current drop of the prepared CuO-60 catalysts at −1.3 V vs. Ag/AgCl, suggesting that CuO is reduced to copper. Smaller differences in current densities of all catalysts at more negative potentials as well as the color change of the catalysts from black to the characteristic reddish-brown color of metallic copper further confirm this hypothesis.

Chemical product analysis during two hours of electrolysis were carried out for all catalysts (5 mg cm^{-2}) at −1.7 V vs. Ag/AgCl under 10 mL min^{-1} CO_2 gas flow. Product formation rates and Faraday efficiencies for C1 compared to C2 and C3 products are shown in Figure 4. More detailed information on the FE for all materials is presented in Table S3 in the Supplementary Material. Among the products, carbon monoxide, formate, ethanol, and n-propanol, besides hydrogen, were detected for all catalyst materials, whereas ethylene was found exclusively for CuO-60 catalysts (Figure 4a). Catalysts Cu-d, Cu-e, and Cu-f, with less oxidized copper species, led to lower hydrocarbon formation rates, especially for alcohols (<0.6 µmol h^{-1} cm^{-2}). However, copper(II) oxide-containing catalysts (CuO-60) showed a distinctly better performance for C2 and C3 product formation with 1.3 to 10.4 µmol h^{-1} cm^{-2} of ethylene, 2.9 to 7.1 µmol h^{-1} cm^{-2} of ethanol, and 1.4 to 5.7 µmol h^{-1} cm^{-2} of n-propanol. Thus, the calcination conditions influence the activity and selectivity of the catalysts toward C2 and C3 products (Figure 4b).

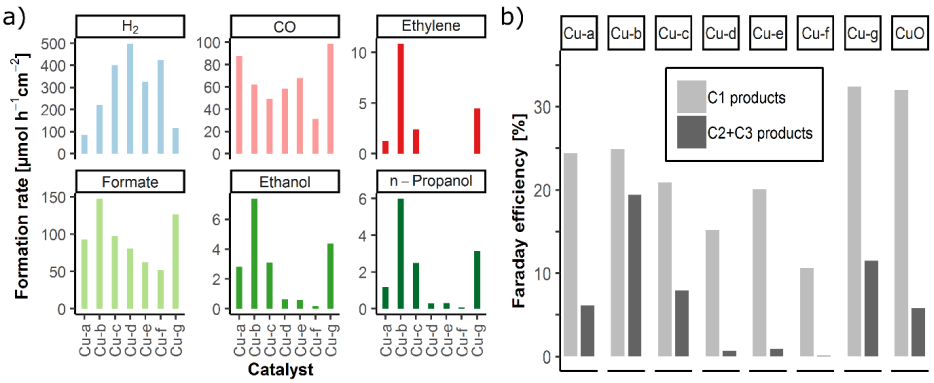

Figure 4. (**a**) Formation rates for hydrogen, carbon monoxide, ethylene, formate, ethanol, and n-propanol for all synthesized copper catalysts at E = −1.7 V vs. Ag/AgCl in CO_2 saturated 0.5 M $KHCO_3$. (**b**) Faraday efficiency of the C1 and C2 + C3 products: significantly increase in C2 and C3 for Cu-b compared to commercial CuO.

The reduction of the CuO obtained from DES calcination to an oxide-derived metallic copper during electrolysis is necessary to create in situ a more active copper modification that promotes the CO_2 reduction to C2 and C3 products. Low amount of CuO domains and higher amounts of metallic copper in the Cu-d, Cu-e, and Cu-f catalysts after DES calcination and before electrolysis may prevent it from achieving the same effect of in situ activation of Cu compared to the CuO-60 catalysts. However, the carbon-rich domains CuO/CNO of these catalysts have similar morphology and show similar electrochemical activity for C1 products, especially formate, consistent with the previous report on CNO rich catalysts [21].

Comparing the different CuO-60 catalysts in more detail, Cu-b and Cu-g show a better performance compared to Cu-a and Cu-c (Figure 4b). Catalyst Cu-b, which was prepared

with the DES Gal-U, shows by far the highest C2 and C3 selectivity. Thus, the change of the DES used for the preparation indicates an influence on catalyst activity and selectivity. Calculation of crystallite sizes by XRD revealed that crystallites of Cu-b and Cu-g are larger in z-direction compared to Cu-a and Cu-c (Table 3). This suggests that a larger z-size of the CuO crystallites is beneficial to the C2 and C3 selectivity in the CO_2 reduction. The performance of the catalysts is in accordance with the findings of various authors [13,33] that the selectivity and efficiency of the copper catalysts is influenced by the crystallite surface areas.

Reproducibility of the experiments was measured for the same batch of the best-performing Cu-b at −1.7 V vs. Ag/AgCl for two runs, as well as two different catalyst batches of Cu-a at the same conditions (Table 4). Apart from hydrogen production, which exhibits a large variation and is mainly responsible for the increase in current density ($\Delta J = 18$ mA cm^{-2} for two runs of the same batch of Cu-b and $\Delta J = 26$ mA cm^{-2} for two different Cu-a batches), the product formation rates of C2 and C3 products (ethylene, ethanol, and n-propanol) have low fluctuations. As for C1 products CO ($\Delta = 13$ µmol h^{-1} cm^{-2} and $\Delta = 44.1$ µmol h^{-1} cm^{-2}) and formate ($\Delta = 16.6$ µmol h^{-1} cm^{-2} and $\Delta = 13.9$ µmol h^{-1} cm^{-2}), these fluctuations are higher, although these remain within the limits of measurement inaccuracies. The total FE differs only by 5% for two runs of the same catalyst Cu-b and by 0.9% for two different Cu-a batches. These results show a good reproducibility for the target products (ethylene, ethanol, and n-propanol) and thus for the catalyst preparation.

Table 4. Product formation rates, Faraday efficiency and current densities for two experiments using the same batch of copper catalyst Cu-b at E = −1.7 V vs. Ag/AgCl in CO_2-saturated 0.5 M $KHCO_3$ and for two different batches of copper catalyst Cu-a.

		Formation Rates [µmol h^{-1} cm^{-2}]						Total FE [%]	*J* [mA cm^{-2}]
		H_2	CO	$HCOO^-$	C_2H_4	C_2H_5OH	C_3H_7OH		
Cu-b	1st run	210.2	59.4	141.1	10.4	7.1	5.7	70.5	−43
	2nd run	373.9	72.4	124.5	13.4	7.5	5.1	65.5	−61
Cu-a	1st batch	252.5	75.3	80.3	3.3	2.5	1.3	54.9	−68
	2nd batch	176.5	119.4	94.2	3.4	3.5	1.8	54.1	−42

Compared to a commercial sample of copper(II) oxide nanoparticles (Figure 4b), the product formation rates of all CuO-60 catalysts, which were prepared by the presented DES calcination in an oxidative atmosphere, increase the selectivity of C2 and C3 products. An influence of calcination temperature on the catalyst selectivity could be excluded by sintering of commercial CuO nanoparticles for one hour at 500 °C. CO_2 reduction on this calcined CuO sample showed lower selectivity toward C2 and C3 products compared to the untreated material. The FE for C2 and C3 products decreased from 5.8% FE for the untreated CuO nanoparticles to 3% FE for the sintered sample. At the same time, it could be confirmed that the DES calcination method improves the selectivity of the prepared catalysts (19.4% FE for C2 and C3 products using Cu-b).

Table 5 shows a comparison of formation rates for C1, C2, and C3 products observed in this work for Cu-b with literature. Cu-b shows high formation rates for C2 and C3 products at a similar potential range compared to literature values. The catalyst shows also very high rates for C1 products (CO and formate).

Table 5. Comparison of the product formation rates from electrochemical CO_2 reduction performed on different electrode materials. E is shown vs. RHE: * converted from −1.7 V vs. Ag/AgCl.

Electrode	E [V]	Formation Rates [μmol h^{-1} cm^{-2}]						Ref.
		CO	$HCOO^-$	CH_4	C_2H_4	C_2H_5OH	C_3H_7OH	
Cu-organic porous materials	−0.90 vs. RHE	-	-	-	-	0.05	-	[34]
Cu-mesocrystals	−0.99 vs. RHE	6	-	-	17	-	-	[35]
Cu-nanocrystals	−1.05 vs. RHE	10	-	-	12	10	2	[36]
CuO/ZnO	−2.5 vs. Ag/AgCl	39.7	-	9.7	1355	?	?	[37]
Cu-b	−1.08 * vs. RHE	59.4	141.1		10.4	7.1	5.7	this work

3. Materials and Methods

3.1. Catalyst Preparation

Catalysts were prepared as described previously [20]. In a round-bottom flask, a total amount of 45 mmol of the DES were heated to 110 °C until a clear, homogeneous liquid was formed. Two different DES were prepared, glucose-urea (Glc-U) in a molar ratio of 2:9 and galactose-urea (Gal-U) 1:7. A defined amount of copper precursor (500 mg copper nanopowder (<100 nm, CuNP) or 650 mg CuO < 50 nm) was added to the DES, and the mixture was heated to 290 °C under air or inert atmosphere for 90 min (pre-treatment). Afterwards, in the calcination step, the pre-pyrolyzed material was heated in a muffle furnace to a final temperature between 450 °C and 550 °C under air for 10, 15, or 60 min, until a fine porous powder was formed. Table 6 shows the detailed synthesis parameters for all catalysts shown in this work.

Table 6. Overview of the different preparation parameter. The following abbreviations correspond to Glc-glucose, Gal-galactose, U-urea, CuNP-copper nanopowder, and RT-room temperature. Cu-e and Cu-f were prepared in two steps: pyrolysis under inert atmosphere and oxidative treatment for 10 min. The measured elemental composition of the catalysts is shown after calcination. Cu-d, Cu-e, and Cu-f show two different types of particles: Cu-rich and Cu-poor ones. The CuO-60 catalysts are Cu-a, Cu-b, Cu-c, and Cu-g.

	Precursor		Pre-Treatment			Calcination			Elemental Composition			
	DES	Metal	*t* [h]	*T* [°C]	Atm.	*t* [min]	*T* [°C]	Atm.	Cu [wt%]	O [wt%]	C [wt%]	N [wt%]
Cu-a	Glc-U	CuNP	1.5	290	air	60	500	air	80.3	13.1	4.4	2.2
Cu-b	Gal-U	CuNP	1.5	290	air	60	500	air	72.8	21.6	3.2	2.5
Cu-c	Glc-U	CuO	1.5	290	air	60	500	air	79.3	14.9	3.5	2.2
Cu-d	Glc-U	CuNP	1.5	290	air	15	500	air	72.9 29.5	14.6 7.0	9.5 48.0	3.2 15.4
Cu-e	Glc-U	CuNP	1.5	290	N_2	from RT 10	to 450 500	N_2 air	62.6 39.2	14.3 4.9	17.0 43.2	6.2 12.7
Cu-f	Glc-U	CuNP	1.5	290	N_2	from RT 10	to 500 550	N_2 air	68.0 49.0	22.8 16.8	5.7 25.9	3.6 8.3
Cu-g	Glc-U	CuNP	1.5	290	N_2	60	500	air	77.1	17.7	2.2	3.0

3.2. Materials Characterization

3.2.1. Scanning Electron Microscopy (SEM)

A scanning electron microscope equipped with secondary electron (SE) energy-dispersive X-ray (EDX) detectors were used to study the morphologies and composition of the materials. Powder samples were fixed on a carbon tape and analyzed using a variable

pressure scanning electron microscope (Leo 1530VP, Zeiss, Oberkochen, Germany) at 15 kV for imaging and EDX.

3.2.2. Powder Diffractometry (XRD)

Materials were assessed by powder X-ray diffractometry in Bragg–Brentano geometry (XRD, Miniflex, Rigaku, Tokyo, Japan, with silicon strip detector D/teX Ultra). Copper K_α radiation with a wavelength λ of 1.54 Å was used, and the samples rotated during measurements. Intensities were recorded in steps of $2\theta = 0.02°$; Soller slits with angular apertures of 5° were used. The maximum recorded scattering angle was $2\theta = 100°$. Samples were placed on monocrystalline silicon substrates, which showed no Bragg reflexes within the considered range of 2θ. Their continuous background scattering intensities were recorded separately and subtracted. The measurements were analyzed by the Rigaku PDXL software (integrated X-ray powder diffraction software, Tokyo, Japan). Therefore, our results were compared with data in the crystallography open database (COD).

A combination with the Scherrer Equation (5) allows the calculation of the crystallite size of copper oxide:

$$Dhkl = \frac{\lambda \cdot \kappa}{FWHM \cdot \cos(\theta)} \quad (5)$$

Thereby, D_{hkl} is the crystallite size in h, k and l direction in reciprocal scale, κ is the shape constant chosen for that system (0.94), and FWHM the full width at half-maximum of the diffraction peak. A detailed calculation of the copper oxide crystallite sizes in real space is shown in Figure S1 in the Supplementary Material.

3.3. Electrochemical Measurements

3.3.1. Electrode Preparation

Here, 5 mg cm^{-2} of the as-prepared catalysts was dispersed in 400 µL of a mixture of distilled water and isopropanol (1:1) containing 10.8 µL of 5 wt% Nafion® solution as binder. The mixture was sonicated for 30 min, drop-coated on the current collectors, and dried at room temperature overnight. The current collectors consisted on 1 cm^2 Toray™ Carbon Paper TP-060 (Quintech, Göppingen, Germany) for cyclic voltammetry (CV) and chronoamperometry (CA) and 3 cm^2 gas-diffusion layers (GDL, Freudenberg, Weinheim, Germany) for experiments with product analysis.

3.3.2. Electrochemical Cells

A one-compartment three electrode cell was used for the first catalyst screening. The current density of all materials was evaluated by CV and CA in 0.5 M $KHCO_3$ electrolyte saturated with CO_2 or Argon. An Ag/AgCl in 3 M KCl electrode (Metrohm, Filderstadt, Germany) was used as reference (RE) and a TiO_2/IrO_2 mesh (Metakem, 6 × 3.5 × 1 × 1 mm, 12 g m^{-2} of Ir, Usingen, Germany) as counter electrode (CE). All experiments were carried out at room temperature (23 °C).

The second step was performed on drop-coated gas-diffusion electrodes (GDE) in a three-compartment cell (Gaskatel, Model: Flexcell PP, Kassel, Germany) comprising an anodic compartment (30 mL of 0.5 M $KHCO_3$), a cathodic side (15 mL of CO_2 saturated 0.5 M KHCO3), and a gas chamber with a constant CO_2 flow of 10 mL min^{-1}. A cation exchange membrane (Fumatech, FUMASEP® FKL-PK-130, Bietigheim-Bissingen, Germany) divided the anode and cathode chamber. Gas (0.6 L gas bags, Sigma Aldrich, Darmstadt, Germany), and liquid samples were collected every 30 min for two hours.

Metrohm Echo Chemie Autolab PGSTAT128N or PGSTAT204 potentiostates (Filderstadt, Germany) controlled by NOVA software (Offenburg, Germany) were used for all electrochemical experiments.

3.4. Product Analysis

3.4.1. Gas Chromatography with Thermal Conductivity Detector (GC-TCD)

The gaseous samples were detected using gas chromatography (GC, Shimadzu 2010, Duisburg, Germany)) equipped with three columns (two Poraplot Q (25 m × 0.53 mm), thickness: 20 µm, one Cp-Molsieve (5A 50 m × 0.53 mm), ID: 50 µm) and a 25 µL sample loop. The temperature program used was 60 °C for 6.3 min followed by a heating rate of 15° min^{-1} to 150 °C and a duration time of 2 min. The thermal conductivity detector (TCD, Shimadzu, Duisburg, Germany) operates under a helium flow of 10 mL min^{-1} at 250 °C, and the product determination was performed using calibration curves for each gaseous product.

3.4.2. Gas Chromatography with Flame Ionization Detector (GC-FID)

The volatile liquid products were detected using a gas chromatography (GC, Shimadzu 2010, Duisburg, Germany) equipped with a Zebron ZB-WAX column (Phenomenex, Aschaffenburg, Germany). The samples were agitated at 90 °C for 15 min, and 2000 µL of the vaporized samples were injected at 250 °C to the equipment. The temperature program used was 35 °C for 7 min followed by a heating rate of 20 °C min^{-1} to 190 °C and a duration time of 3 min with a helium column flow of 1 mL min^{-1}. Quantification was performed using calibration curves.

3.4.3. High-Pressure Liquid Chromatography (HPLC)

The acidic product determination was performed using high-pressure liquid chromatography (HPLC, Shimadzu LC20A, Duisburg, Germany) with a Rezex ROA-organic acid H+ (8%) column (Phenomenex, Aschaffenburg, Germany). For formate determination, an isocratic separation with 0.005 N H_2SO_4 was used with a flow of 0.5 mL min^{-1}. Quantification was done using calibration curves. For that, a sample of 150 µL was taken during the process, and 10 µL were injected at the equipment.

3.4.4. NMR Spectroscopy

NMR spectroscopy was carried out in a JEOL JNM ECA 400 MHz spectrometer (Jeol, Freising, Germany). For the experiments, the following parameter were used: 25 °C, 90° pulse, NS of 128, relaxation time of 18 s, and water suppression of 40 DB. The internal standard 3-(trimethylsilyl) propanoic acid sodium salt-D4 dissolved in deuterium oxide was used for product quantification.

4. Conclusions

The reported protocol demonstrates a promising, novel, and facile preparation method for carbon-containing copper oxide electrocatalysts based on deep eutectic solvent calcination, which show a remarkable performance for C2 and C3 products from electrochemical CO_2 reduction. The catalyst properties were affected by the preparation parameters such as type of DES and copper precursor or the treatment time in air during calcination. Copper precursors influence the morphology of the catalyst particles, and the type of DES affects the crystallite size of copper in *z*-direction. Time of oxidative thermal treatment influences the oxidation state of copper and the amount of supporting material CNO formed from the DES. Thermal treatment for 60 min in air provides exclusively copper(II) oxide-containing catalysts with less carbonaceous support, while shorter time causes less oxidized forms of copper (Cu_2O and Cu^0), besides CuO and distinctly higher amounts of support.

Electrochemical investigations of the catalysts revealed that calcination at 500 °C in air for 60 min leads to higher activity and C2/C3 product selectivity compared to shorter treatment times. Moreover, copper(II) oxide is reduced to metallic copper at an early stage of the CO_2 reduction experiment, which has an intrinsic influence on the catalytic performance of the in situ-formed oxide-derived copper species.

The catalyst prepared with the DES Gal-U, copper nanoparticles as precursor and an oxidative treatment for 60 min at 500 °C showed the highest activity and enhanced

the selectivity toward C2 and C3 products significantly compared to commercial CuO. This catalyst produced 141.1 µmol h^{-1} cm^{-2} formate, 10.4 µmol h^{-1} cm^{-2} ethylene, 7.1 µmol h^{-1} cm^{-2} ethanol, 5.7 µmol h^{-1} cm^{-2} n-propanol, and 59.4 µmol h^{-1} cm^{-2} CO at −1.7 V vs. Ag/AgCl at the investigated optimum process parameters 5 mg cm^{-2} catalyst loading, 10 mL min^{-1} CO_2 gas flow in 0.5 M $KHCO_3$.

Supplementary Materials: The following are available online at https://www.mdpi.com/article/10.3390/catal11050542/s1, Figure S1: Scheme of the monoclinic CuO crystallite. Axes h, k and l are orthogonal to the planes, spanned by unity cell axes a, b and c. Figure S2: SEM images of synthesized copper materials comprising light (+) and dark (−) particle types. CuO/AC shows CuO mixed with activated carbon (commercial products). Figure S3: SEM images of all synthesized copper materials and CuO/AC. Figure S4: X-ray powder diffractograms of all copper catalysts show different copper oxidation states (0, + I and + II). The measurements are normalized to 1. Figure S5: Formation rate of hydrogen, carbon monoxide, ethylene, formate, ethanol and n-propanol for different CO_2 flows and Cu-a catalyst loadings for two hours. The experiments were performed at constant potential E = −1.7 V vs. Ag/AgCl in CO_2 saturated 0.5 M $KHCO_3$., Figure S6: Products generated by the copper catalyst Cu-g between −2.1 V, −1.9 V, −1.7 V and −1.5 V in CO_2 saturated 0.5 M $KHCO_3$ electrolyte. The measurements were performed for half an hour at each potential., Figure S7: Overview of the current densities at −1.7 V vs. Ag/AgCl. The 0.1 M concentrated electrolyte degrades after ~ 40 min, while the 0.5 M $KHCO_3$ is stable for about 120 min., Figure S8: Chronoamperograms for synthesized copper catalysts in Argon and CO_2 saturated 0.5 M $KHCO_3$. Potentials shown vs. Ag/AgCl., Table S1: Increase of pH during 2 h reaction time., Table S2: Total product formation rates for 2 h reaction time using copper catalyst Cu-a in two different concentrated $KHCO_3$ electrolytes at E = −1.7 V vs. Ag/AgCl., Table S3: Faraday efficiencies of all synthesized copper materials at E = −1.7 V vs. Ag/AgCl in CO_2 saturated 0.5 M $KHCO_3$. In this table more detailed information of Figure 4b is shown.

Author Contributions: Funding acquisition, V.S., T.G.; investigation and experimental work, M.I. and J.S.; methodology, M.I., L.V., M.K. and D.V.O.; project administration and resources L.V.; software, D.V.O.; supervision, L.V., C.Z., T.G., M.R. and B.K. writing—original draft, M.I.; writing—review & editing, J.S., L.V., C.Z., T.G., B.K. and V.S. All authors have read and agreed to the published version of the manuscript.

Funding: Financial support of this work by the Bavarian Ministry of Economic Affairs and Media, Energy and Technology and the Center of Energy Storage and the Fraunhofer "Leitprojekt Strom als Rohstoffquelle" is acknowledged.

Data Availability Statement: The data presented in this study are available on request from the corresponding author.

Conflicts of Interest: The authors declare no conflict of interest.

References

1. Indermühle, A.; Monnin, E.; Stauffer, B.; Stocker, T.F.; Wahlen, M. Atmospheric CO_2 concentration from 60 to 20 kyr BP from the Taylor Dome Ice Core, Antarctica. *Geophys. Res. Lett.* **2000**, *27*, 735–738. [CrossRef]
2. Benson, S.M.; Orr, F.M. Carbon Dioxide Capture and Storage. *MRS Bull.* **2008**, *33*, 303–305. [CrossRef]
3. Rahman, F.A.; Aziz, M.A.; Saidur, R.; Abu Bakar, W.A.W.; Hainin, M.; Putrajaya, R.; Hassan, N.A. Pollution to solution: Capture and sequestration of carbon dioxide (CO_2) and its utilization as a renewable energy source for a sustainable future. *Renew. Sustain. Energy Rev.* **2017**, *71*, 112–126. [CrossRef]
4. Leung, D.Y.C.; Caramanna, G.; Maroto-Valer, M.M. An overview of current status of carbon dioxide capture and storage technologies. *Renew. Sustain. Energy Rev.* **2014**, *39*, 426–443. [CrossRef]
5. Olajire, A.A. CO_2 capture and separation technologies for end-of-pipe applications—A review. *Energy* **2010**, *35*, 2610–2628. [CrossRef]
6. "Molly" Jhong, H.-R.; Ma, S.; Kenis, P.J. Electrochemical conversion of CO_2 to useful chemicals: Current status, remaining challenges, and future opportunities. *Curr. Opin. Chem. Eng.* **2013**, *2*, 191–199. [CrossRef]
7. Kumar, B.; Brian, J.P.; Atla, V.; Kumari, S.; Bertram, K.A.; White, R.T.; Spurgeon, J.M. New trends in the development of heterogeneous catalysts for electrochemical CO_2 reduction. *Catal. Today* **2016**, *270*, 19–30. [CrossRef]

8. Whipple, D.T.; Kenis, P.J.A. Prospects of CO_2 Utilization via Direct Heterogeneous Electrochemical Reduction. *J. Phys. Chem. Lett.* **2010**, *1*, 3451–3458. [CrossRef]
9. Azuma, M.; Hashimoto, K.; Hiramoto, M.; Watanabe, M.; Sakata, T. Carbon dioxide reduction at low temperature on various metal electrodes. *J. Electroanal. Chem. Interfacial Electrochem.* **1989**, *260*, 441–445. [CrossRef]
10. Hori, Y.; Murata, A.; Takahashi, R.; Suzuki, S. Enhanced formation of ethylene and alcohols at ambient temperature and pressure in electrochemical reduction of carbon dioxide at a copper electrode. *J. Chem. Soc. Chem. Commun.* **1988**, *1*, 17–19. [CrossRef]
11. Gawande, M.B.; Goswami, A.; Felpin, F.-X.; Asefa, T.; Huang, X.; Silva, R.; Zou, X.; Zboril, R.; Varma, R.S. Cu and Cu-Based Nanoparticles: Synthesis and Applications in Catalysis. *Chem. Rev.* **2016**, *116*, 3722–3811. [CrossRef]
12. Roberts, F.S.; Kuhl, K.P.; Nilsson, A. High Selectivity for Ethylene from Carbon Dioxide Reduction over Copper Nanocube Electrocatalysts. *Angew. Chem. Int. Ed.* **2015**, *54*, 5179–5182. [CrossRef]
13. Ren, D.; Deng, Y.; Handoko, A.D.; Chen, C.S.; Malkhandi, S.; Yeo, B.S. Selective Electrochemical Reduction of Carbon Dioxide to Ethylene and Ethanol on Copper(I) Oxide Catalysts. *ACS Catal.* **2015**, *5*, 2814–2821. [CrossRef]
14. Loiudice, A.; Lobaccaro, P.; Kamali, E.A.; Thao, T.; Huang, B.H.; Ager, J.W.; Buonsanti, R. Tailoring Copper Nanocrystals towards C2 Products in Electrochemical CO_2 Reduction. *Angew. Chem. Int. Ed.* **2016**, *55*, 5789–5792. [CrossRef]
15. Kim, D.; Kley, C.S.; Li, Y.; Yang, P. Copper nanoparticle ensembles for selective electroreduction of CO_2 to C_2–C_3 products. *Proc. Natl. Acad. Sci. USA* **2017**, *114*, 10560–10565. [CrossRef]
16. Li, C.W.; Kanan, M.W. CO_2 Reduction at Low Overpotential on Cu Electrodes Resulting from the Reduction of Thick Cu_2O Films. *J. Am. Chem. Soc.* **2012**, *134*, 7231–7234. [CrossRef] [PubMed]
17. Kuhl, K.P.; Cave, E.R.; Abram, D.N.; Jaramillo, T.F. New insights into the electrochemical reduction of carbon dioxide on metallic copper surfaces. *Energy Environ. Sci.* **2012**, *5*, 7050–7059. [CrossRef]
18. Hori, Y. Electrochemical CO_2 Reduction on Metal Electrodes. In *Modern Aspects of Electrochemistry*; Vayenas, C.G., White, R.E., Gamboa-Aldeco, M.E., Eds.; Springer: New York, NY, USA, 2008; pp. 89–189.
19. Zhang, W.; Hu, Y.; Ma, L.; Zhu, G.; Wang, Y.; Xue, X.; Chen, R.; Yang, S.; Jin, Z. Progress and Perspective of Electrocatalytic CO2Reduction for Renewable Carbonaceous Fuels and Chemicals. *Adv. Sci.* **2018**, *5*, 1700275. [CrossRef] [PubMed]
20. Iwanow, M.; Finkelmeyer, J.; Söldner, A.; Kaiser, M.; Gärtner, T.; Sieber, V.; König, B. Preparation of Supported Palladium Catalysts using Deep Eutectic Solvents. *Chem. A Eur. J.* **2017**, *23*, 12467–12470. [CrossRef] [PubMed]
21. Iwanow, M.; Vieira, L.; Rud, I.; Seidler, J.; Kaiser, M.; Van Opdenbosch, D.; Zollfrank, C.; Richter, M.; Gärtner, T.; König, B.; et al. Pyrolysis of Deep Eutectic Solvents for the Preparation of Supported Copper Electrocatalysts. *Chemestry* **2020**, *5*, 11714–11720. [CrossRef]
22. Muniz, F.T.L.; Miranda, M.A.R.; Dos Santos, C.M.; Sasaki, J.M. The Scherrer equation and the dynamical theory of X-ray diffraction. *Acta Crystallogr. Sect. A Found. Adv.* **2016**, *72*, 385–390. [CrossRef]
23. Wagle, D.V.; Zhao, H.; Baker, G.A. Deep Eutectic Solvents: Sustainable Media for Nanoscale and Functional Materials. *Accounts Chem. Res.* **2014**, *47*, 2299–2308. [CrossRef] [PubMed]
24. Gattrell, M.; Gupta, N.; Co, A. A review of the aqueous electrochemical reduction of CO_2 to hydrocarbons at copper. *J. Electroanal. Chem.* **2006**, *594*, 1–19. [CrossRef]
25. Hori, Y.; Takahashi, R.; Yoshinami, A.Y.; Murata, A. Electrochemical Reduction of CO at a Copper Electrode. *J. Phys. Chem. B* **1997**, *101*, 7075–7081. [CrossRef]
26. Wojtowicz, J.A. The carbonate system in swimming pool water. *J. Swim. Pool Spa Ind.* **2001**, *4*, 54–59.
27. Lum, Y.; Yue, B.; Lobaccaro, P.; Bell, A.T.; Ager, J.W. Optimizing C–C Coupling on Oxide-Derived Copper Catalysts for Electrochemical CO_2 Reduction. *J. Phys. Chem. C* **2017**, *121*, 14191–14203. [CrossRef]
28. Lum, Y.; Ager, J.W. Stability of Residual Oxides in Oxide-Derived Copper Catalysts for Electrochemical CO_2 Reduction Investigated with 18 O Labeling. *Angew. Chem. Int. Ed.* **2018**, *57*, 551–554. [CrossRef]
29. Nitopi, S.; Bertheussen, E.; Scott, S.B.; Liu, X.; Engstfeld, A.K.; Horch, S.; Seger, B.; Stephens, I.E.L.; Chan, K.; Hahn, C.; et al. Progress and Perspectives of Electrochemical CO_2 Reduction on Copper in Aqueous Electrolyte. *Chem. Rev.* **2019**, *119*, 7610–7672. [CrossRef] [PubMed]
30. Handoko, A.D.; Chan, K.W.; Yeo, B.S. –CH_3 Mediated Pathway for the Electroreduction of CO_2 to Ethane and Ethanol on Thick Oxide-Derived Copper Catalysts at Low Overpotentials. *ACS Energy Lett.* **2017**, *2*, 2103–2109. [CrossRef]
31. Zheng, Y.; Vasileff, A.; Zhou, X.; Jiao, Y.; Jaroniec, M.; Qiao, S.-Z. Understanding the Roadmap for Electrochemical Reduction of CO_2 to Multi-Carbon Oxygenates and Hydrocarbons on Copper-Based Catalysts. *J. Am. Chem. Soc.* **2019**, *141*, 7646–7659. [CrossRef]
32. Pander, J.E.; Ren, D.; Huang, Y.; Loo, N.W.X.; Hong, S.H.L.; Yeo, B.S. Understanding the Heterogeneous Electrocatalytic Reduction of Carbon Dioxide on Oxide-Derived Catalysts. *ChemElectroChem* **2018**, *5*, 219–237. [CrossRef]
33. Kas, R.; Kortlever, R.; Milbrat, A.; Koper, M.T.M.; Mul, G.; Baltrusaitis, J. Electrochemical CO_2 reduction on Cu_2O-derived copper nanoparticles: Controlling the catalytic selectivity of hydrocarbons. *Phys. Chem. Chem. Phys.* **2014**, *16*, 12194–12201. [CrossRef]
34. Albo, J.; Vallejo, D.; Beobide, G.; Castillo, O.; Castaño, P.; Irabien, A. Copper-Based Metal-Organic Porous Materials for CO_2 Electrocatalytic Reduction to Alcohols. *ChemSusChem* **2017**, *10*, 1100–1109. [CrossRef] [PubMed]
35. Chen, C.S.; Handoko, A.D.; Wan, J.H.; Ma, L.; Ren, D.; Yeo, B.S. Stable and selective electrochemical reduction of carbon dioxide to ethylene on copper mesocrystals. *Catal. Sci. Technol.* **2014**, *5*, 161–168. [CrossRef]

36. Ren, D.; Wong, N.T.; Handoko, A.D.; Huang, Y.; Yeo, B.S. Mechanistic Insights into the Enhanced Activity and Stability of Agglomerated Cu Nanocrystals for the Electrochemical Reduction of Carbon Dioxide to n-Propanol. *J. Phys. Chem. Lett.* **2016**, *7*, 20–24. [CrossRef] [PubMed]
37. Merino-Garcia, I.; Albo, J.; Solla-Gullón, J.; Montiel, V.; Irabien, A. Cu oxide/ZnO-based surfaces for a selective ethylene production from gas-phase CO_2 electroconversion. *J. CO_2 Util.* **2019**, *31*, 135–142. [CrossRef]